UNIVERSITÀ DEGLI STUDI DI PADOVA

Dipartimento di Fisica e Astronomia "Galileo Galilei"

Degree in Physics

Final Dissertation

Study of the H_α emission of the SPIDER negative ions source

Thesis supervisor

Dr. Matteo Agostini

Candidate

Francesco Franco

Academic Year 2020/2021

Abstract

This dissertation assesses and compares plasma behaviour under different configurations of the **plasma grid magnetic filter** in the **SPIDER** experiment, part of the larger ITER project, through the study of the H_α emission of the hydrogen plasma.

ITER is an international collaboration, involving the European Union, China, India, Japan, Korea, Russia and the United States, whose objective is to demonstrate the feasibility of fusion power generation through plasma magnetic confinement. A low density hydrogen plasma will be heated to about $1.5 \cdot 10^8$ K to start the nuclear fusion reaction. The project design will allow a self-sustaining process for long-duration machine runs (up to 1 h) to reach the 500 MW of fusion power output goal [1]. Many systems and subsystems are needed to reach such a high temperature: together with ohmic heating, thermal energy will be fed to the plasma via microwave radiation and neutral particle scattering, provided by two neutral beam injectors (NBI).

The **SPIDER** ion source is part of the NBI system, providing up to 60 A current of H^- ions extracted from a hydrogen plasma. Ions are then accelerated up to 100 keV and neutralised to obtain a high intensity neutral beam [2].
However, to achieve the required specification to ignite nuclear fusion and obtain the best power output, all systems need to achieve maximum optimisation.

In the specific case of **SPIDER**, efficiency is achieved by maximising the spatial homogeneity of the neutral beam, which, in-turn, depends on the uniformity of the plasma produced in the source, which is required to deviate less than $\pm 10\%$ from ideal uniformity [2]. Many of **SPIDER** source components are still being tuned to solve stability and homogeneity issues, as well to increase the negative ions production. Thus, the study of the effects of the PG magnetic field topology on the produced plasma is of great interest to obtain the required data to improve plasma uniformity.

In this dissertation, the **SPIDER** plasma source is introduced, along with the components of interest of this study, namely the **plasma grid magnetic filter**, in two topological configurations: a first prototype and a second improved one, and the plasma generators. Data analysis is then outlined presenting labelling, analysis roadmap and methodology. Finally, results assessment and description is conducted to lead to the final data comparison across different analysis methods.

Contents

Chapter 1

Introduction

The **SPIDER** plasma source is composed of eight drivers arranged in a two-by-four grid (approx. 1 m × 2 m) [3]. Construction details of each driver can be seen in the Figure 1.1. Drivers are then organised in four RF (radio-frequency) generators, each one feeding two drivers (left-right coupling), connected to a RF power feed. In front of the open side of the plasma source a vertical metal grid is placed, named **plasma grid** (PG), as a first negative ions extraction step. The grid features 1280 holes - arranged in 16 groups (4 × 4) consisting of 5 holes (horizontally) × 16 holes (vertically) - through which negative ion beamlets are extracted using the potential gradient between the plasma grid and the so called **extraction grid**, placed in parallel to the plasma grid further on. Acceleration of each beamlet ensues by applying a second electric field between the extraction grid and the **grounded grid**, situated down the line. Co-extracted electrons are dumped on the extraction grid itself with permanent magnets. Compensation for ion deviations due to the magnetic field is achieved with a second set of permanent magnets on the grounded grid. To minimise the electron density and temperature in front of the plasma grid in order to improve the negative ions lifetime, a magnetic filter is used: a current is run through the plasma grid in the vertical direction, thus creating a transverse magnetic field in front of the grid.

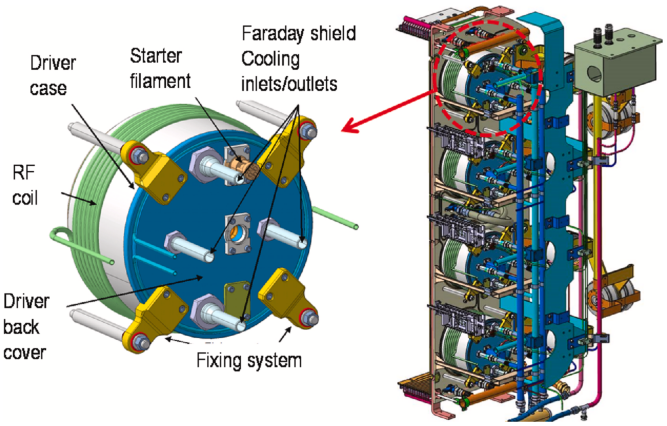

Figure 1.1: A render of a **SPIDER** driver.

The plasma grid magnetic filter decreases the density and temperature of electrons extracted together with the negative ions, thus increasing the chances of successful H^- extraction and lifetime.
However, the PG magnetic filter is known to also affect plasma behaviour inside the source and, consequently, its spatial homogeneity. Indeed, the magnetic filter topology is characterised by the plasma grid current density and the return busbar geometry. Hence, plasma characterisation allows to asses the impact of different solutions for the plasma grid magnetic filter.

In particular, this contribution focuses on characterising plasma production - in relation to other working parameters of the experiment - with two different magnetic filter configurations which, for the sake of this dissertation, will be named:

- **Original** magnetic configuration: the first implemented geometry presents a single copper busbar, running along the the centre-back of the generator assembly from top to bottom. However, this solution was observed to be causing plasma weakening, and following turn-off, above a certain threshold of the PG current in conjunction with other experimental parameters, such as source pressure and RF power. This is interpreted as an in-driver electron loss due to the

magnetic field itself;

- **Optimised** magnetic configuration: this new configuration of the power supply adds to the original configuration three parallel copper busbars, placed behind the generator assembly, running form the top to the bottom of the machine. This optimised current sharing allows to maintain the same field at the PG, while reducing its effects inside the source [4] [5].

1.1 Data introduction

The following analysis will focus on various parameters:

• **plasma light** (PL), the H_α photon flux signal coming from each individual driver [3][6], measured by a photodiode in

$$\left[\frac{n_\gamma}{\Sigma \cdot t}\right] = \mathrm{m}^{-2}\mathrm{s}^{-1}$$

(where n_γ is the number of incoming photons, Σ is the detection area of the sensor and t is the sampling time interval), related to plasma production rate as it depends on electron density. Indeed, the light intensity measured is proportional to

$$I_{H_\alpha} \propto (n_e\, n_n)\, \sigma$$

in which n_e is the electron density, n_n the neutral atoms density and σ is the process cross-section.

Each of the 8 total plasma light photodiodes, labelled as PL_i $i = 1, \ldots, 8$, measures the intensity of the H_α emission inside a single driver. As Figure 1.2 shows, each PL_i is numbered from top to bottom and left to right. Couples of drivers are assigned to a group, numbered from 1 to 4 starting from the top, and they are referred to as **generators**, as each couple is independently controlled. To ease readability, each group, or generator, is assigned to a shade of colour. Hence, each PL is colour coded accordingly to the respective group to maintain a consistent visual clue while comparing quantities in the same generator.
• **RF power** of each generator, labelled by group GR_i $i = 1, 2, 3, 4$ starting from the top of the source;
• **vessel pressure** (PR), measured in mPa, the hydrogen gas pressure measured nearby the source. The analysis focuses on a single probe located inside the containment vacuum vessel and pressure is measured as gas diffuses outside and around the experiment within the chamber. As such, pressure measuring does not resolve single drivers, but returns an overall value;
• **plasma grid current** (PG), measured in kA.

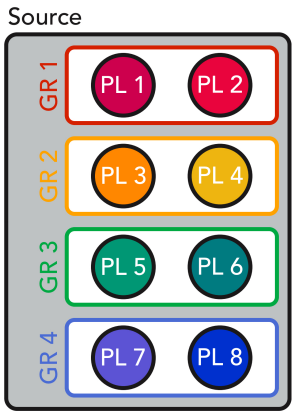

Figure 1.2: Labelling criteria of the 8 drivers and 4 RF groups.

Since this analysis is focused on assessing the uniformity of the plasma produced, it will verify its homogeneity on two different directions, namely the left-right direction and the top-bottom direction. In particular, the H_α intensity ratio among couples of PL values PL_i/PL_j is calculated, since it indicates uneven plasma production in different areas of the source. Furthermore, data analysis involves two complementary methods.

The **data bulk** approach compiles a great amount of data obtained by a total of 420 experimental runs. Each of them is characterised by stable experimental parameters. Data is averaged over the longest available time interval that comply to the stability request. In the example Figure 1.3, each group data has been individually gathered on the stable plateau of each plasma ignition. The collection of many data points with different experimental setups allows to compose a wider plasma

behaviour assessment. It must be noted that the bulk approach surveys in one picture many experimental scenarios, some in which all generators are running at the same time, some in which each generator is working alone and all combinations in between.

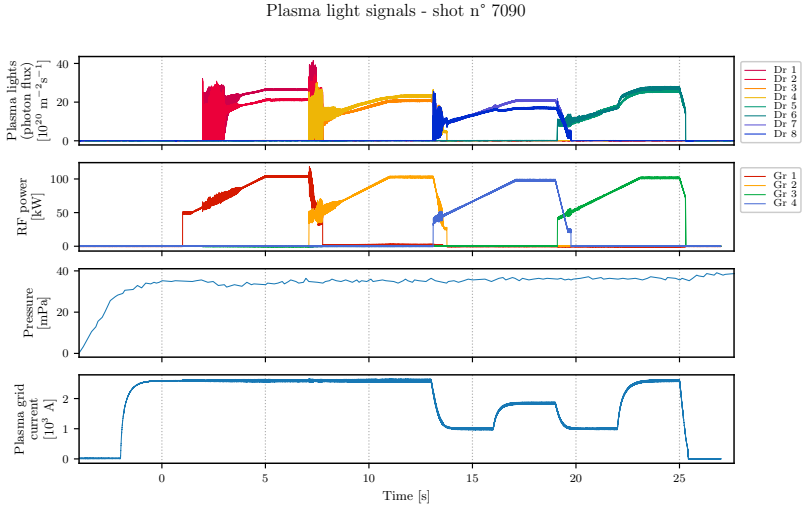

Figure 1.3: Example of a bulk run using the optimised PG configuration. In the top panel, each plasma light signal is plotted according to the labelling criteria shown in Figure 1.2. Plasma lights sequentially switch on, increase and turn off group by group. In the second plot, RF power of each group is represented. Pulse activation of each group leads to plasma ignition, as the PL signals show. In this example, groups are activated in the following order: 1 (red), 2 (yellow), 4 (blue) and 3 (green). The mutual interaction between RF power and plasma can be seen at each group activation. The third and last panels show respectively the pressure inside the vessel and the PG current.

Complementarily, the **ramp signal** approach focuses on much fewer shots that present a regular increase, or decrease, of PG current and, for further development, RF power, hence the name "ramp" for a single, smooth and continuous variation of parameters. In Figure 1.4, three sawtooth-like PG ramps can be seen, each one with matching constant RF value, offering the possibility of multiple scans.

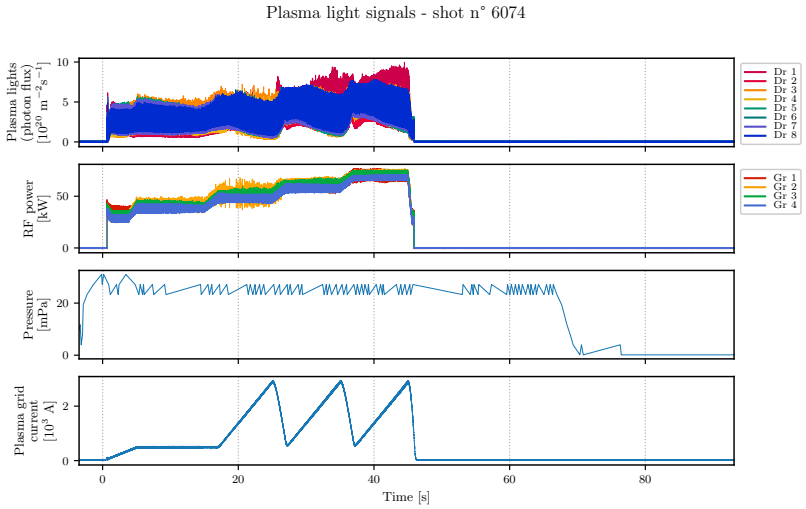

Figure 1.4: Example of a multiple-ramp run using the original configuration of the PG (generator n°4 in blue highlighted for clarity). In the top figure, all plasma light signals are active at the same time, colour coded as shown in Figure 1.2. RF power is represented in the second plot as it increases in all groups at the same time. The third plot represents the pressure inside the vessel. The last graph shows the PG current as it increases in three sawtooth-like ramps.

In order to analyse ramp experimental runs, data has been averaged over 1 s intervals in the area of interest, assuming plasma characteristic response time to be much shorter than any varying parameter. However, this assumption is not far fetched, as experimental signals show negligible delay between the

machine parameter change and the PL response. Furthermore, this assumption is also proven by the results of this analysis.

1.1.1 Comments about errors

As seen in Figure 1.3 and 1.4, plasma light appears to fluctuate. It must be noted that this kind of phenomenon is not due to noise, indeed, it is a still unassessed phenomena concerning the mutual interaction between the RF pulse and the plasma itself, as also the RF power signals can be seen fluctuating. The H_α emission intensity oscillates with a specific frequency not explainable by the RF characteristic frequency (about 1 MHz), for it is much slower, but may be due to beats inside the plasma. Indeed, in Figure 1.4 all groups are active at the same time and PL signal carries a much more pronounced oscillation compared to the one seen in Figure 1.3, when only one group is active at a time. Thus, a mutual interaction involving plasma and RF feed may be the explanation of such phenomena. This also may imply that the plasma inside a single driver could be influenced by the RF of adjacent drivers. Moreover, electronic noise can be sampled from the H_α signal at the end of the experimental run. At most, its halfwidth can be estimated to be $5 \cdot 10^{18}$ $m^{-2}s^{-1}$, negligible compared to the measured signal. Furthermore, plasma fluctuations represent a phenomena with a much shorter characteristic time compared to the overall phenomena involving the macroscopic variation of experimental parameters. The main goal of this contribution is to identify possible general relations between the factors at play, hence it will not assess errors which are to considered irrelevant.

Chapter 2

Analysis of plasma uniformity

Before introducing the analysis results, some notation is presented. For a given time interval Δt, for each experimental parameter the **mean** is calculated and denoted with μ_i, where i is referred to a single parameter, e.g. $i = \mathrm{PL}_1, \ldots, \mathrm{PL}_8; \mathrm{GR}_1, \ldots, \mathrm{GR}_4; \mathrm{PR}; \mathrm{PG}$.

2.1 Left-right uniformity in the data bulk

2.1.1 Original magnetic configuration runs

The original magnetic configuration bulk data set presents a more prominent plasma instability. The original magnetic topology was observed to present a blind spot, close to the driver walls, which caused electron loss, a flaw detrimental to the plasma, that leads to plasma shutdown above the 3 kA filter current mark at higher RF power [4]. This fact forced a lowering of RF power - beyond which plasma instability would disrupt the source activity - settling the RF power of the majority of experimental runs to 60 kW.
Data bulk results with the original magnetic configuration are shown in Figure 2.1. The left-right uniformity of plasma is studied group by group by calculating the ratio of the averaged PL values of adjacent drivers. A single point represents the result of a single experimental run. In clockwise order, starting from the top-left plot, the uniformity of the first group is shown. In the top left-hand driver (PL_1), H_α intensity is higher than the one on the right side (PL_2), as the signal ratio rarely goes below 1. A remarkable dependency on the PG current can be seen: as the PG increases, the emission intensity consistently shits on the left. Moving down the source, groups GR_2, GR_3 and GR_4 do show a less prominent dependency on the PG filter current. Furthermore, GR_2 and GR_4 are very close to 1, indicating a quite uniform plasma emission across the group. GR_3, instead, has higher intensity on the right-hand driver (PL_6), and increasing non-uniformity as the PG increases.

Upon closer look, a RF dependency may be identified, as the majority of data points with lower RF values (in lighter colour) tend to lay in the lower section of the plot, suggesting a left-right asymmetry among drivers that depends on RF power.

A third-order polynomial fit of the data

$$\frac{\mu_{\mathrm{PL}_i}}{\mu_{\mathrm{PL}_j}}(I) = a_0 + a_1 I + a_2 I^2 + a_3 I^3$$

has been added to provide visual guidance, it also helps to assign proper weight to the abundant data clusters, which provide a more stable insight on the plasma source activity in certain regions.

It is also suggested that RF fields may interact with plasma across drivers. Indeed, data of GR_2 and GR_3, that are in the middle of the source, show more coherent and less spread trends. Their reciprocal influence, probably due to RF fields overlapping, helps to stabilise and homogenise plasma production, resulting in similar behaviours and a closer to one ratio. Furthermore, extremal groups, namely GR_1

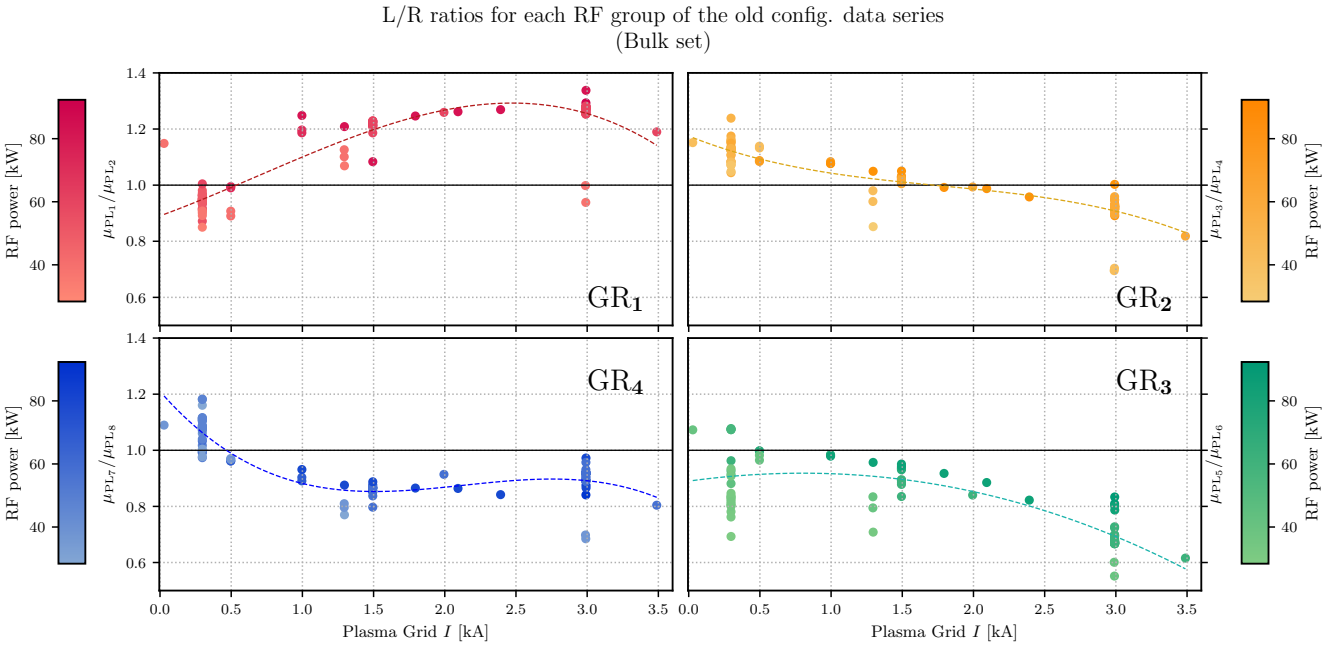

Figure 2.1: Original configuration data bulk results. In clockwise order, starting from the top left corner, Groups 1, 2, 3 and 4 are plotted. Each coloured point represents the ratio of adjacent averaged PL signals of each group, denoted with μ_{PL_i}, where $i = 1, \ldots, 8$ refers to each driver. Shade variation encodes the RF power of each run. GR_1 (red) ratio is shifted to the left, a reinforcing trend as PG increases. GR_2 (yellow) and GR_4 (blue) are almost uniform in their left-right intensity and do not present a strong dependence on the PG. GR_3 (green) has higher intensity on the right-hand side, also reinforcing as PG increases.

and GR_4, shall carry a more pronounced instability and unbound trends. Indeed, GR_1 plot stands out amongst the other groups for its peculiar trend.

2.1.2 Optimised magnetic configuration runs

Figure 2.2 shows the data bulk left-right homogeneity results using the optimised magnetic filter topology (implementing the additional busbars geometry). Each point represents a single experimental run, namely the ratio of the averaged PL signals of the left-hand and right-hand driver of each group. As shown, GR_1 slightly depends on the PG, as for GR_3. However, while GR_3 lays closer to the 1 mark, showing a plasma uniformity, GR_1 shows a predominant left-hand intensity, as the ratio consistently settles around 1.2.

The ratio of groups GR_2 and GR_4 is quite close to 1 as well, thus presenting a plasma left-right homogeneity without any relevant PG-related trend. However, groups 1 and 4, respectively the top and bottom generators, show a larger data dispersion, which might indicate that the lack of other surrounding groups leads to unbound and more non uniform plasma emission. However, it must be noted that the improved magnetic field produced by the optimised plasma grid allows to work at high RF power supply, shifting the majority of the data points around the 100 kW mark. This, in turn, allows to produce higher plasma density, hence it must be considered that, especially for GR_1 and GR_4, such ratio values - similar to the original configurations - might have been unobtainable.

2.2 Left-right uniformity in ramp signals

In this section the the left-right asymmetry in ramp discharges is discussed. Different ramps in different configurations have been studied and two different exemplary cases of interest are presented: a run where all drivers are active and one in which only GR_1 is working. An additional example is then introduced to study the effect of RF power on the H_α intensity in respect to constant PG current values and pressures.

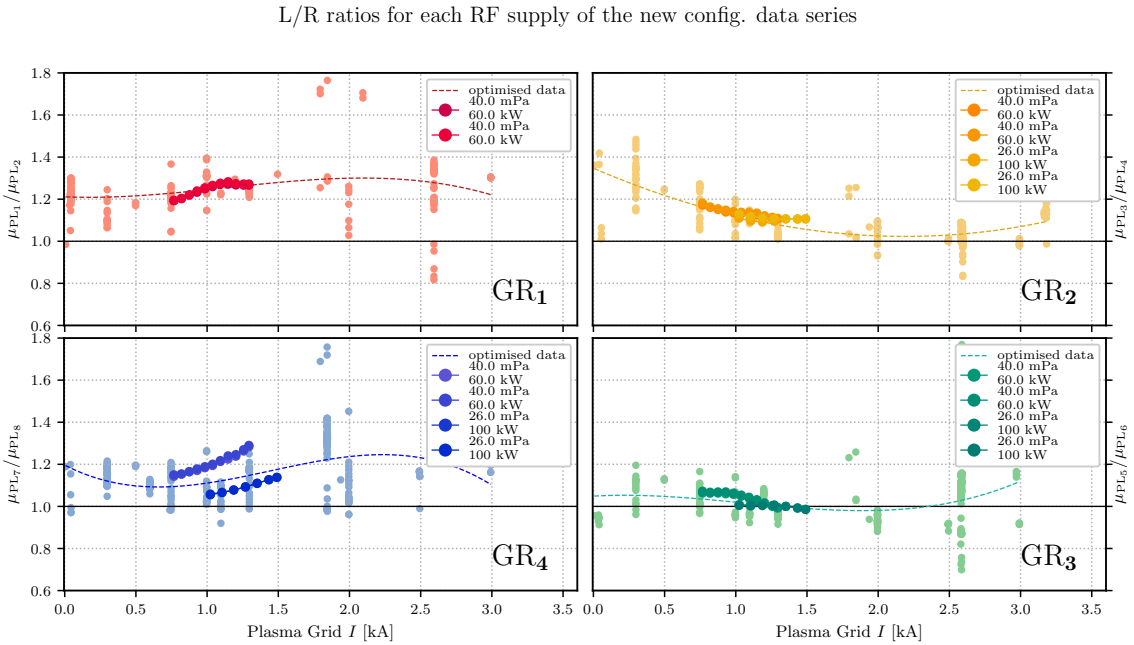

Figure 2.2: Optimised configuration global data results. In clockwise order, starting from the top left corner, Groups 1, 2, 3 and 4 are plotted. The ramps results (connected points) are laid over the bulk points (scattered and light coloured). Each point is the left-right ratio of averaged PL signals of each driver couple. In the case of the bulk points, the average value is calculated over the longest time interval in which parameters are constant. In the case of the ramp data, the average is calculated over 1 s intervals along the ramp.

2.2.1 Original magnetic configuration runs

In this first example, reported in Figure 2.3, GR_1 is the only active group. Each point on a single curve is the ratio of PL signals averaged over 1 s intervals along the ramp. This plot is the result of the analysis of 6 consecutive PG ramps, 3 increasing and 3 decreasing, each one scanning different pressure and RF settings. For the sake of clarity, ramps with different RF values have been split into two distinct plots in the figure. The overall PG trend is consistent throughout the whole run, as well as the tendency of higher RF values data sets to populate plot regions with higher ratio values, as seen in Figure 2.1. This confirms a global asymmetry in the machine, as the left-hand side increases light intensity as RF increases. The effects of pressure can be seen, as ramps at a lower pressure result in a more pronounced non-homogeneity. Keeping RF constant, as pressure increases, data trends approach the 1 value, while lower pressure values lead to an increased non-uniformity (bottom two curves). This is, however, expected, as larger pressure may smooth local density fluctuations, resulting in a closer-to-1 ratio value. However, these single-group runs present much different trends compared to the data bulk in Figure 2.1, a phenomena observed as well in shots n° 6048 and 6050 (where GR_2 is the only active one).

In this case, the ratio follows a trend with the PG current with two bends, as it first decreases, then increases to finally decrease again, while, in the data bulk, group 1 ratio presents an overall constantly increasing trend. This may be due to the already suggested mutual interaction among RF fields: the plasma behaviour in a group changes according to the neighbouring groups activity.

In Figure 2.4 all four generators are working at the same time. The three data curves shown overlaid to the data bulk represent three distinct PG ramps in the shot n° 6074. Each point refers to the PL (averaged over 1 second intervals) left-right ratio of each group. In this case, ramp trends match quite closely the one of the bulk, suggesting that the parallel activity of multiple generators changes the overall behaviour of plasma.
The effects of the RF power is studied in Figure 2.5. Setting constant PG current and pressure and linearly increasing RF power, the averaged plasma light signal in each group (over 1 s intervals along the RF ramp) has been used to calculate the left-right ratio of each generator. GR_1 consistently

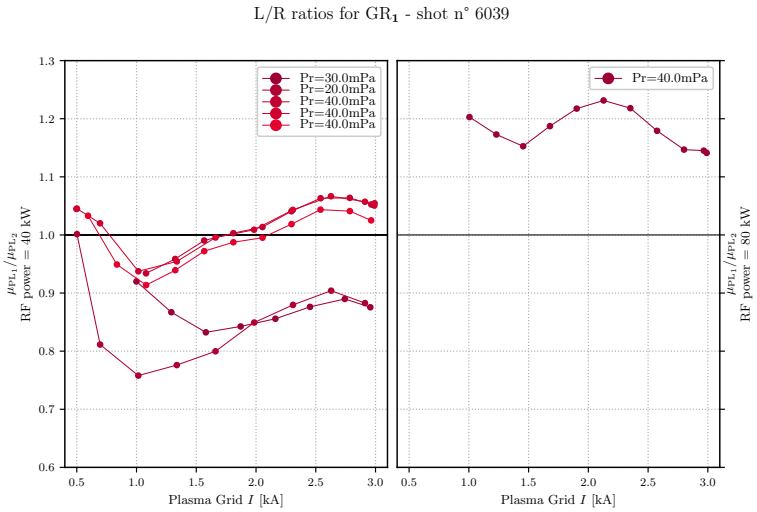

Figure 2.3: Original configuration shot (with multiple ramps) with generator 1 running solo (drivers 1 and 2). Each point represents the ratio of PL signals of the two drivers, averaged over a 1 s interval. Different curves refer to different ramps, each capturing different machine parameters, labelled on the plot, namely the pressure, as it increases ramp by ramp, and the RF power, set to two different values (40 kW on the left and 80 kW on the right). For the sake of clarity, the two RF data families have been split into two plots.

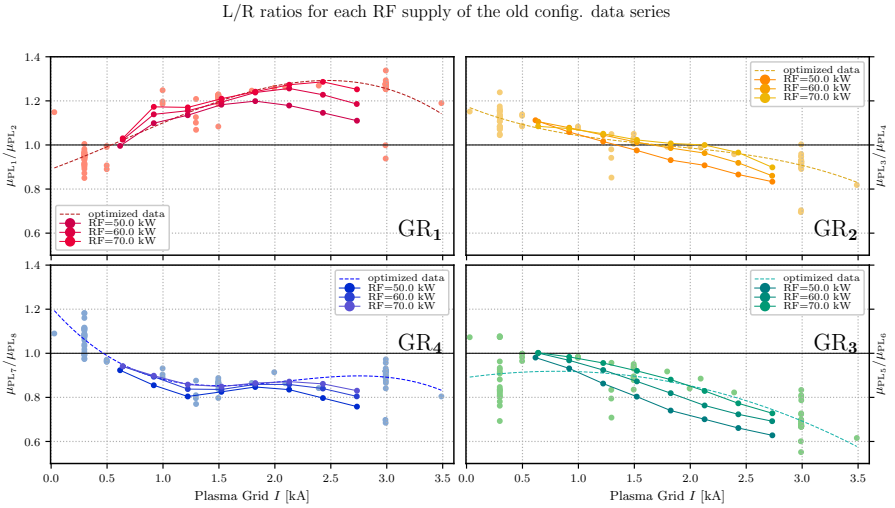

Figure 2.4: Original configuration global data results. In clockwise order, starting from the top left corner, Groups 1, 2, 3 and 4 are plotted. The ramps results (connected points) are laid over the bulk points (scattered and light coloured). Each point is the left-right ratio of averaged PL signals of each generator driver couple. Colour coding follows from Figure 1.2. In all four plots, the ramp trend matches the bulk one as long as all four generators are active at the same time.

rises above 1, implying that the intensity in left-hand driver is higher as RF increases. On the other hand, GR$_2$ settles around the 1 threshold, thus presenting a good plasma uniformity across drivers 3 and 4. Moreover, the ratio increases up to 60 kW, then, for larger RF power, it carries a saturation trend. The same behaviour is shared with GR$_3$, confirming the idea that central groups influence and stabilise each other by proximity, although its right-hand driver has a higher light intensity as the PL ratio never rises above 1. Finally, GR$_4$ shares the same trend with GR$_1$, confirming that outer groups which have an open side (respectively, group 1 the top part and group 4 the bottom part) behave differently. However, plasma intensity in GR$_4$ is more predominant on the right-hand side, as the ratio is consistently lower than 1 in the whole RF power range, and increasing RF power brings uniformity to the plasma emission as data approaches 1.

2.2.2 Optimised magnetic configuration runs

All the optimised magnetic configuration ramps (respectively, shots n° 7328, 7331, 7747 and 7748) involve multiple groups running simultaneously. In fact, with the exception of shots n° 7747 and 7748, where GR_1 is turned off, all groups are active at the same time.

In these cases, a narrower PG value interval is scanned. As shown in Figure 2.2, these ramp curves present two different RF values: 60 kW and 100 kW. While in groups 2 and 3 the two RF power show a similar behaviour, as a clear separation between the two RF families can not be seen, in group 4 datas with different RF settings can be recognised. This may be due to the electromagnetic locking of adjacent inner groups, namely GR_2 and GR_3 as their activity results very similar due to reciprocal influence. Instead, group 4 may behave differently as it lacks a neighbouring generator on the bottom part. However, the splitting due to different RF power is much less visible, indicating an increased stability of the source. The optimised magnetic configuration brought many improvements to the plasma behaviour, as ramp curves confirm a lesser homogeneity dependency on the PG current, for relevant trends as the PG increases are not easily identifiable.

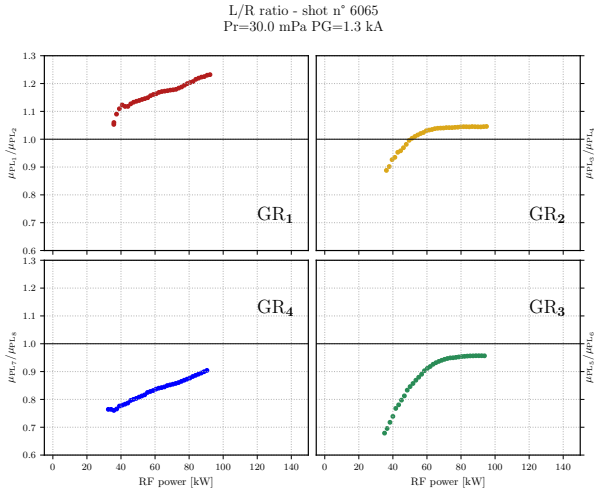

Figure 2.5: Original configuration shot with a single RF rising ramp with constant pressure and PG. Each point represents the ratio of PL signals of the two drivers, averaged over a 1 s interval.

2.3 Top-bottom uniformity

In the following section, the vertical uniformity of the H_α light intensity is characterised, comparing its emission between the top and bottom outer groups (GR_1 and GR_4) and inner groups (GR_2 and GR_3). Therefore, in a similar fashion to the left-right homogeneity study, the ratio of the average plasma light intensity of couples of drivers is calculated. For the data bulk, the average is taken over the longest available time interval that complies to the stability requirement of parameters. For ramp shots, the average is calculated over 1 s intervals along PG ramps. Indeed, the data used in the left-right analysis is suitable for this comparison upon further selection, so that compared data across different groups presents compatible RF power. Therefore, the following results refer to the filtered data bulk, the shot n° 6074 for the original configuration ramps and shots n° 7328 and 7331 for the optimised configuration ramps.

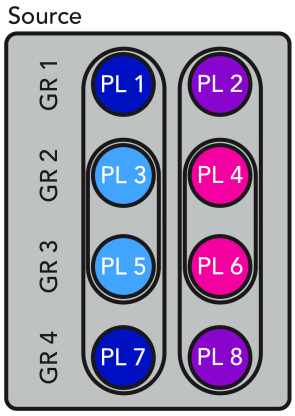

Figure 2.6: Labelling criteria of the 8 drivers and 4 RF groups according to the top-bottom analysis criteria.

The analysis thus compares the following: PL_1 and PL_7 (outer groups 1 and 4, on the left-hand side), PL_2 and PL_8 (outer groups 1 and 4, on the right-hand side), PL_3 and PL_5 (inner groups 2 and 3, on the left-hand side) and PL_4 and PL_6 (inner groups 2 and 3, on the right-hand side). The colour coding and labelling is shown in Figure 2.6. Note that non-uniformities across the vertical direction indicate two different plasma density gradients: indeed, outer groups 1 and 4 are 3 times more spaced out than the inner groups 2 and 3, thus uniformities along the top-bottom direction account for density gradient over different distances.

2.3.1 Original magnetic configuration runs

In Figure 2.7, light coloured scattered points refer to the plasma light ratios of the data bulk of each driver pair, while ramp ratio results are overlaid as connected points. Starting from the top-left panel, in clockwise order, the following pairs ratios are plotted: PL_1 and PL_7 (outer groups 1 and 4, on the left-hand side), PL_2 and PL_8 (outer groups 1 and 4, on the right-hand side), PL_3 and PL_5 (inner groups 2 and 3, on the left-hand side) and PL_4 and PL_6 (inner groups 2 and 3, on the right-hand side). Ramp data curves match quite closely the data bulk. However, behaviour-wise, the ratio of PL_1 and PL_7, in the top-left panel, stands out amongst the other pairs. Indeed, its trend is similar to the one assessed in the left-right analysis for group 1 using the original configuration. Other ratios (respectively, in clockwise order, outer right drivers, inner right drivers and inner left drivers) show a less prominent dependency on the PG, as their trend does not present large variations across the PG range. Moreover, the ratio of the right-hand side of the source (two right-hand panels in pink) mostly lays below 1, indicating a higher intensity in the bottom half of the generator array as PL_4 and PL_8 result stronger. As stated, even though these two ratios are similar, they refer to much different density gradients as the non-uniformity in the outer groups (top panels) is spread out over 3 times the distance of the inner drivers (bottom panels). However, taking into consideration the left-right analysis for the group 1 with the original magnetic configuration, the parabolic trend of both ratios $\frac{PL_1}{PL_2}$ and $\frac{PL_1}{PL_7}$ may be due to a peculiar behaviour of the driver 1 in respect to the others, whose plasma light intensity strongly depends on the PG magnetic field, thus influencing both the left-right and top-bottom homogeneity.

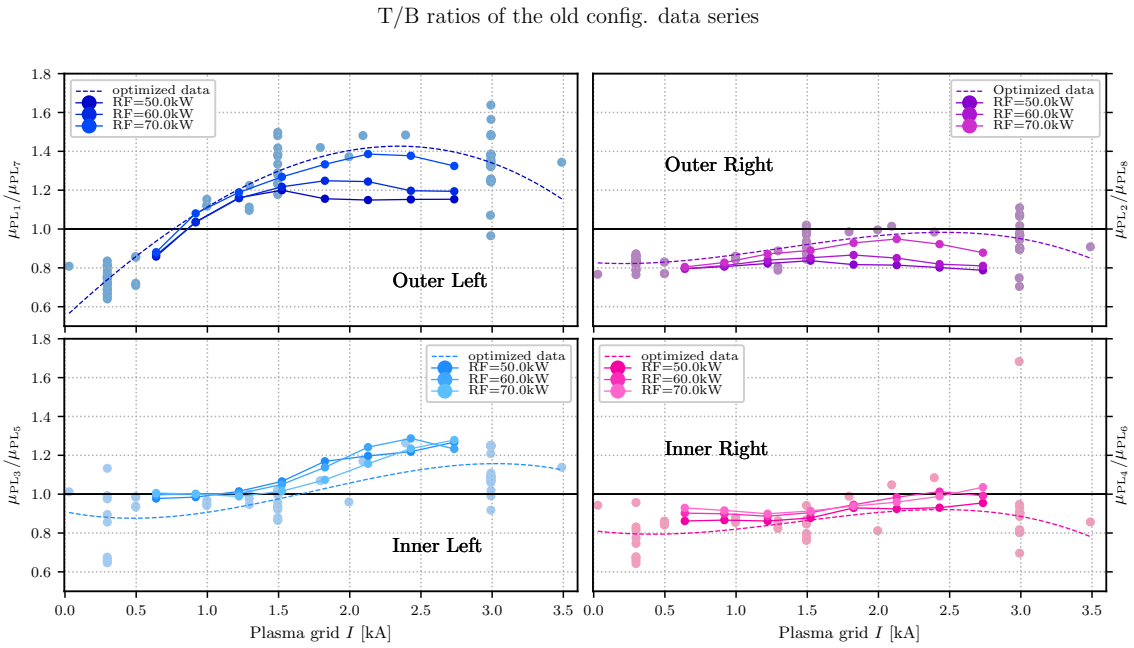

Figure 2.7: Original configuration global data results. In clockwise order, starting from the top left corner, outer groups 1 and 4 on the left-hand side, outer groups 1 and 4 on the right-hand side, inner groups 2 and 3 on the left-hand side and inner groups 2 and 3 on the right-hand side. Colour coding follows from Figure 2.6. In the case of the bulk points (scattered points), the average value is calculated over the longest time interval in which parameters are constant. In the case of the ramp data (connected points), the average is calculated over 1 s intervals along the ramp. The three ramp curves have distinct constant RF values. In all four plots, the ramp trend matches the bulk one.

2.3.2 Optimised magnetic configuration runs

With the optimised magnetic filter configuration, in Figure 2.8, ratio values are overall close to 1 (except for the inner right drivers (bottom right panel), PL_4 and PL_6, which remain below 1, indicating a higher intensity of PL_6). Some trends can be identified in respect to the outer groups (top two panels). Indeed, the plasma light ratio (respectively, $\frac{PL_1}{PL_7}$ on the left and $\frac{PL_2}{PL_8}$ on the right) gets closer to 1 as the PG current increases. However, the strong dependence on the PG of the outer left drivers

has disappeared, as also seen previously in the the left-right analysis, confirming the beneficiary effect of the optimised PG geometry in respect the the original one.

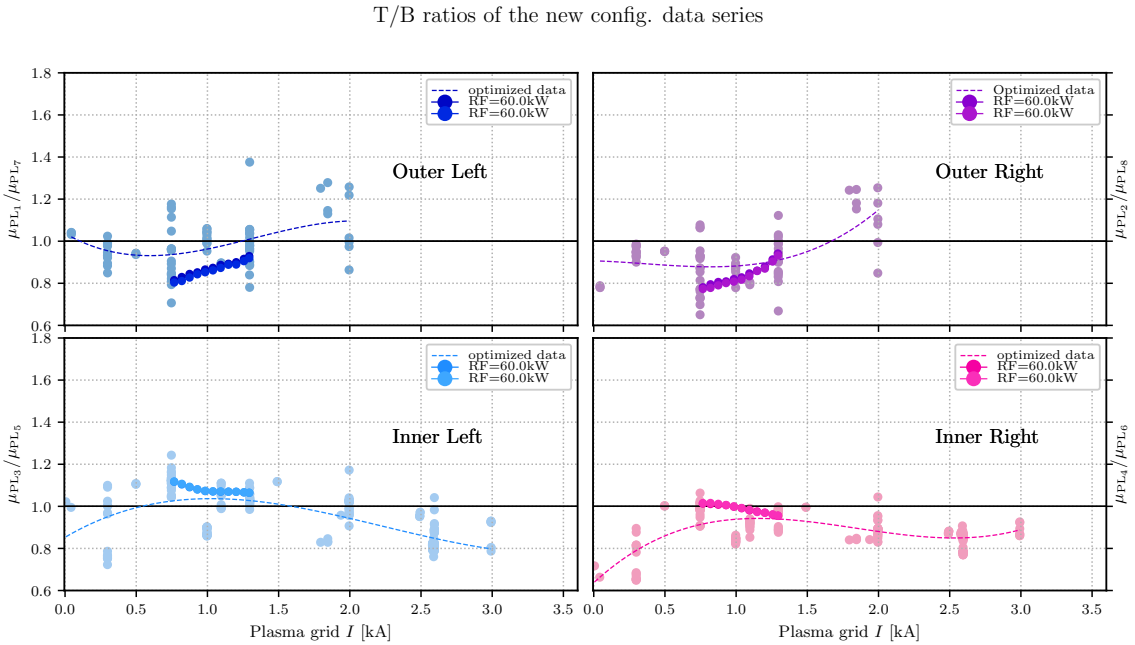

Figure 2.8: Optimised configuration global data results. In clockwise order, starting from the top left corner, outer groups 1 and 4 on the left-hand side, outer groups 1 and 4 on the right-hand side, inner groups 2 and 3 on the left-hand side and inner groups 2 and 3 on the right-hand side. Colour coding follows from Figure 2.6. The three ramp curves have distinct constant RF values. In all four plots, the ramp trend matches the bulk one. Ramp data may not be easily distinguished as the almost exactly overlap.

Chapter 3

Conclusions

In this thesis, the effects of magnetic filter field of the plasma grid (PG) on the uniformity of the plasma of the **SPIDER** negative ions source has been characterised. In particular, the different impact of two PG designs has been assessed.

The original design of the plasma grid introduced plasma inhomogeneity, which depends on the flowing current along the grid. Figure 2.1 shows a particularly strong dependence of the left-right uniformity on the PG in group 1 (top-left panel), as well as group 3 (bottom-right panel) which reinforces as the PG current increases. A less pronounced trend can be identified in the two remaining groups 2 and 4. Dependence on the radio-frequency power is also assessed, as Figure 2.1 presents a gradient where data ratios with lower RF lays in the lower part of the graph, while higher RF values result in higher ratios. This is confirmed by the left-right ramp analysis in Figure 2.4, whose trends match the bulk ones in terms of PG current and RF power.

Moreover, the top-bottom homogeneity assessment for the original configuration shows a peculiar behaviour of the plasma light 1 (driver 1, topmost-left of the driver array [3][6]), as its light emission dependency on the PG current similarly impacts both on the left-right ratio in group 1 (thus PL_1 and PL_2) and the top-bottom ratio between groups 1 and 4 on the left side (PL_1 and PL_7).

Since the non-uniformity of the plasma inside the source could lead to to a non-uniform ion beam, this issue is overcame with the optimised plasma grid geometry in order to reduce the penetration of the filter magnetic field inside the drivers.

The optimised configuration brought many improvements to the plasma source, as Figure 2.2 does not present a strong dependency on the PG, much more pronounced in Figure 2.4. Looking at Figure 2.2, both bulk and ramp data ratios lay closer to 1, with less obvious trends as the H_α intensity is less dependent of the PG across all four generators, confirming that the optimised configuration allows to increase the magnetic filter strength, thus reducing co-extracted electrons, without causing excessive non-uniformities inside the source. The optimised field topology provides a more localised effect around the plasma grid, reducing perturbations inside drivers.

Moreover, the ramp shots confirm the uniformity improvement for group 2 and group 3, as the ratios of H_α emissivity on between left and right drivers approaches 1.

In light of the top-bottom homogeneity analysis, the reduced influence of the plasma grid magnetic field, due to the optimised configuration, is confirmed, as Figures 2.7 and 2.8 show a much weaker dependency of the plasma intensity on the PG current. Moreover, the new PG configuration has minimized the peculiar behaviour of driver 1, whose H_α emission showed the strongest dependence on the PG current respect to the other drivers.

It must be noted that, with the use of the original geometry, while the left-right homogeneity shows a dependency on the PG current, the top-bottom analysis does not show clear trends (with the exception of PL_1). This implies that the transverse plasma grid magnetic field affects the horizontal uniformity

of the plasma (along the magnetic field direction), impacting much less on the top-bottom distribution. This effect is smoothed with the new geometry, which influences much less the light intensity across all drivers and directions.

Therefore, the optimised plasma grid magnetic filter topology is confirmed to improve the plasma source performance: plasma light ratios are closer to 1 along left-right and top-bottom directions, thus bringing a homogeneity improvement, and their variation is much less pronounced as the plasma grid magnetic field changes, thus showing a reliability enhancement.

References

[1] *The ITER Organization official website*. URL: https://www.iter.org.

[2] V. Toigo et al. "Progress in the ITER neutral beam test facility". In: *Nuclear Fusion* 59 (2019), p. 086058. DOI: 10.1088/1741-4326/ab2271.

[3] G. Serianni et al. "First operation in SPIDER and the path to complete MITICA". In: *Review of Scientific Instruments* 91 (2020), pp. 1–8. DOI: 10.1063/1.5133076.

[4] A. Pimazzoni et al. "Co-extracted electrons and beam inhomogeneity in the large negative ion source SPIDER". In: *Fusion Engineering and Design* 168 (2021), p. 112440. DOI: 10.1016/j.fusengdes.2021.112440.

[5] N. Marconato et al. "An optimized and flexible configuration for the magnetic filter in the SPIDER experiment". In: *Fusion Engineering and Design* 166 (2021), p. 112281. DOI: 10.1016/j.fusengdes.2021.112281.

[6] B. Zaniol et al. "First measurements of optical emission spectroscopy on SPIDER negative ion source". In: *Review of Scientific Instruments* 91 (2020), p. 013103. DOI: 10.1063/1.5128900.

Ringraziamenti

Un ringraziamento speciale va al mio relatore di tesi, Dr. Matteo Agostini, per la sua preziosa guida nell'elaborazione di questo lavoro. Ho trovato di ispirazione la sua passione per la ricerca in corso e il suo approccio sinergico alla fisica sperimentale, conferma di quanto questa attività sia entusiasmante, nella scoperta di fenomeni e nell'avanzamento di conoscenze, un passo alla volta. Ringrazio il Prof. Gianluigi Serianni per i suoi insegnamenti in aula e per il prezioso feedback fornito durante l'attività di analisi ed interpretazione dei dati, e tutta la squadra di lavoro all'IGI, il cui entusiasmo per l'avanzamento della ricerca nella fusione nucleare è stata la carica nel mio lavoro.
Ringrazio i miei amici e colleghi di questi anni di studio per tutto il supporto e consiglio, tra cui c'è anche quello di lavorare alla tesi nella squadra di SPIDER, consiglio il cui valore non dimenticherò.
Dedico poi un ringraziamento speciale ai miei amici Orso e Maria, che rimangono per me esempi di dedizione scientifica da seguire, per l'ispirazione e il supporto datomi in questi anni.
Infine, un grande grazie va a mio papà e mia mia mamma, ai miei fratelli, ai nonni e alla mia famiglia tutta per essere sempre stati al mio fianco e per aver sempre creduto nel mio percorso e nella mia passione. Non solo, anche per aver sopportato, come spesso capita a chi abbia uno scienziato in casa, diversi discorsi su tematiche settoriali difficilmente comprensibili ai non addetti (ma, dopotutto, ognuno deve avere i suoi sfoghi). Un grazie a chiunque sia stato partecipe di questo capitolo della mia vita e abbia contribuito a rendere speciale questo traguardo.